ELSEVIER

Journal of Structural Geology 26 (2004) 1157–1171

JOURNAL OF STRUCTURAL GEOLOGY

www.elsevier.com/locate/jsg

Fluid flow in extensional environments; numerical modelling with an application to Hamersley iron ores

J.G. McLellan[a,b,*], N.H.S. Oliver[a,b], P.M. Schaubs[c,d]

[a]*Economic Geology Research Unit, James Cook University, Townsville, Qld 4811, Australia*
[b]*Predictive Mineral Discovery, Co-operative Research Centre, James Cook University, Townsville, QLD 4811, Australia*
[c]*Predictive Mineral Discovery, Co-operative Research Centre, CSIRO EM, Kensington, WA 6151, Australia*
[d]*CSIRO, Exploration and Mining, Kensington, WA 6151, Australia*

Received 1 November 2002; received in revised form 1 June 2003; accepted 2 July 2003

Abstract

The mechanical feasibility of focusing both surface- and basinal-derived fluids towards sites of iron ore genesis during Proterozoic deformation in the Hamersley Province is tested here by computer simulation. Finite difference modelling of porous media flow during extensional deformation of a mountain range shows that surface fluids are drawn towards areas of failure and focus into the centre of the mountain. The addition of permeable structures such as a normal fault provides focused fluid pathways in which mechanical and geological conditions are particularly conducive to both upward and downward flow. Upward flow from the base of the fault within the model overall is favoured by low permeability basement materials and supra-hydrostatic pore pressures. Downward migration of fluids becomes more prominent as extension progresses and upward fluid flow from the base diminishes. The introduction of sedimentary layering into the models allows lateral fluid flow, such that sites of potential fluid mixing may then occur within permeable iron formation units close to the fault zone. Allowing parts of the stratigraphy to become more permeable as a function of high fluid flux simulates permeability enhancement by silica dissolution as a mechanism for iron ore genesis. The involvement of both basinal and surficial fluids in the genesis of the ore deposits is supported by the mechanical models and in addition provides an explanation for a progression from relatively reduced to oxidised conditions at the Mt Tom Price deposit (and possibly other large deposits) with time.

Keywords: Numerical modelling; Fluid flow; Extension; Hamersley Province; Banded iron formations

1. Introduction

Surface fluids have been implicated in subsurface ore forming processes in several geologic environments (e.g. Epithermal: Sillitoe, 1993; Mississippi Valley Type (MVT): Garven, 1985). Surface fluids moving downwards during sedimentation may become overpressured or underpressured during the burial–compaction–inversion cycle of sedimentary basins and compacting basins can generate abnormal fluid pressures or overpressurised zones (Bredehoeft and Hanshaw, 1968; Kissen, 1978; Bethke, 1985; Neuzil, 1995). Strongly inverted basins with elevated mountain ranges may also be dominated by topographically driven fluid flow (Fig. 1). Regional groundwater flow studies with applications to hydrologic, petroleum and mineral systems have been examined previously (e.g. Tóth, 1962, 1963; Freeze and Witherspoon, 1966; Garven and Freeze, 1984a,b; Oliver, 1986; Upton et al., 1995), and these studies recognise the varying effects of topography and deformation in controlling hydraulic head gradients and hence the migration of fluids within the crust. Compaction driven or overpressurised upward flow is a common feature in the generation of hydrocarbon deposits (e.g. Upton et al., 1998) and within sedimentary basins (Bethke, 1985), and has also been related to fault activity (Sibson, 1987; Sibson et al., 1988). Lateral fluid flow is generally influenced by topography and the permeability of geological units, where topographic influences on the hydraulic head have been shown to drive fluid in a downward and lateral direction. For example, Tóth (1962, 1963), Garven and Freeze (1984a) and Nesbitt and Muehlenbachs (1989) have interpreted that deep gravity-driven flow has significant implications for large-crustal hydrodynamic processes. For contractional deformation, Oliver (1986) has described the 'squeegee' effect of thrusts enabling considerable lateral fluid flow and the potential for mixing of surficial and deep-seated fluids during this process. Downward migration of fluids has been attributed to underpressure, or as a result of extensional deformation, where vertical interconnectivity of fractures

* Corresponding author. Tel.: +61-7-4871-6438; fax: +61-7-4725-1501.
E-mail address: john.mclellan@jcu.edu.au (J.G. McLellan).

0191-8141/$ - see front matter © 2004 Elsevier Ltd. All rights reserved.
doi:10.1016/j.jsg.2003.11.015

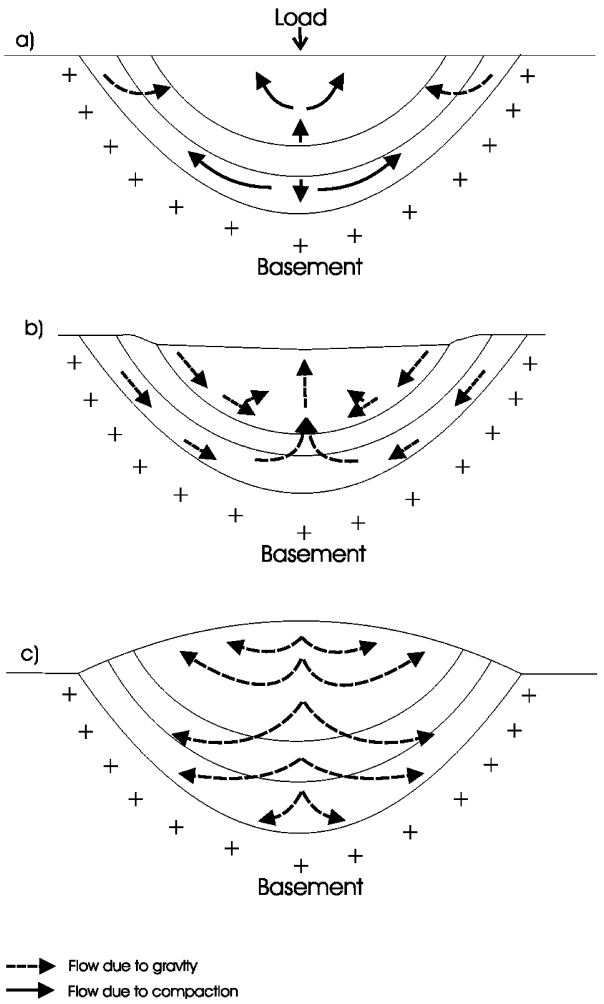

Fig. 1. Hydrological cycles for (a) compacting basin, (b) mature basin, and (c) topographical systems (adapted from Domenico and Schwartz, 1997).

within rocks allows deep penetration of surface fluids (Nesbitt and Muehlenbachs, 1989). Deformation induced fluid flow has been discussed by several authors (Etheridge et al., 1983, 1984; Oliver, 1996; Oliver et al, 2001; Ord and Oliver, 1997; Cox, 1999) and this process undoubtedly has great influence over directions and rates of flow, particularly at depth.

Sedimentary basins are subjected to several forces that are known to cause large-scale fluid migration (Garven and Raffensperger, 1997), which include gravity, thermal and chemical buoyancy, compaction, loading, unloading, dilation, and overpressurisation. Large-scale flow has been linked to many types of ore deposits e.g. Mississippi Valley Type (MVT) deposits, and fluid modelling has shown that flow can be as great as 1 to 10 m yr^{-1} when associated with topographic driven flow in a foreland basin (Garven and Raffensperger, 1997). Within these low temperature environments the process of fluid mixing has been proposed for many different types of ore deposits (e.g. Kendrick et al., 2002a,b; Sharpe and Gemmell, 2002), and in some circumstances evidence of downward meteoric water incursion has been linked to later oxidising stages of ore formation. However, the nature of fluid flow that may allow localisation of ore deposits is primarily controlled by the permeability and porosity of the rocks. Dissolution and cementation are two processes that can alter the permeability of any given rock, fracture or vein. The process of dissolution allows increased fluid flux and hence increasing fluid pathways and the potential to carry dissolved metals, which are of great concern in forming ore deposits, excellent examples being carbonate-hosted MVT deposits.

The basic theory of fluid flow has been realised since the time of Hubbert (1940), although the patterns of flow within porous media can change dramatically as a result of hydraulic head, pressure, structure, heat and mineralogical variations. Numerical models of fluid flow at depth have been utilised for many geological scenarios (e.g. Upton et al., 1995, 1998; Ord and Oliver, 1997; Koons et al., 1998; Upton, 1998; Oliver et al., 1999, 2001; Gow et al., 2002; Ord et al., 2002; Schaubs and Zhao, 2002), and have become an important tool for simulating the response of geological materials and fluid flow to deformation. In this paper we examine the effects of topography, structure, extension and permeability creation on fluid flow within a collapsing mountain range. These modelling scenarios are applied to the structural setting and ore genesis of the Hamersley Province, Western Australia, but in a generic form could be applied to many other extensional environments worldwide, particularly in the 2 to 8 km-depth range of deep sedimentary basins and the shallow parts of orogenic belts.

2. Hamersley Province

The Hamersley Province is located in the southern part of the Pilbara Craton, Western Australia (Fig. 2) and covers an area of approximately 40,000 km^2. It consists of an Archean granite–greenstone basement overlain by Archaean to Paleo-Proterozoic volcanoclastic-sedimentary packages (Mt Bruce Supergroup), which are divided into three main groups: Fortescue Group, Hamersley Group and the Turee Creek Group. In the southern part of the province the Hamersley Group hosts some of the world's largest iron ore deposits, Mt Whaleback, Mt Tom Price and Paraburdoo, which are all mineralogically distinctive in displaying abundant hematite of microplaty and martite varieties with minor goethite. These deposits are hosted mainly in the Dales Gorge Member, which away from ore consists of banded iron formation (BIF) with interbedded shale layers (Trendall and Blockley, 1970; Harmsworth et al., 1990). These microplaty hematite deposits are characterised by extremely high grades (>60% Fe), high porosity (5–50%), and lack of silica. Mt Whaleback, the largest deposit in the region, is surrounded by low–medium temperature quartz veins (100–300 °C fluid inclusion homogenisation temperatures), some of which may be relevant to ore genesis (Brown et al., 2004).

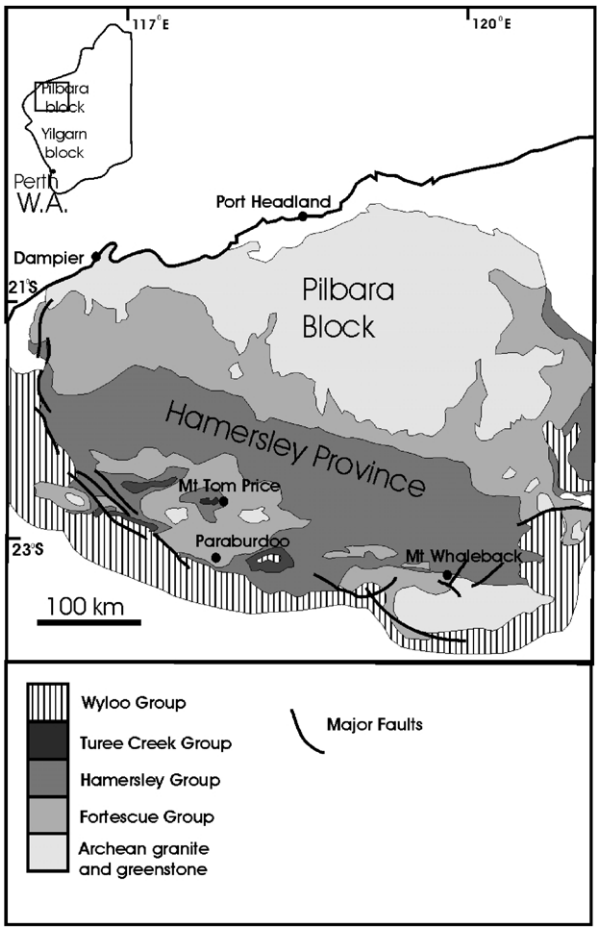

Fig. 2. Simplified regional geological map and summary of stratigraphic groups (modified from Li et al., 1993).

2.1. Structural history

Major structural contrasts can be seen between the northern and southern regions of the Hamersley Province The northern region is markedly less deformed than the southern region and is characterised by shallow open folds trending N–NW. More intense deformation occurred in the southern region as a result of the collision between the Yilgarn and Pilbara blocks (Tyler and Thorne, 1990; Martin et al., 1998), and this is characterised by open folds in the SW and tighter E–W-trending folds in the SE. The Ophthalmian (ca. 2450–2200 Ma) and the Capricorn Orogenies (ca. 1820–1650 Ma) are the two main deformational events to have affected the province (Tyler and Thorne, 1990; Powell et al., 1998). The dominant folding event throughout the southern region (F_2) is a result of the Ophthalmian Orogeny and this major event was associated with thrusting and shear zone development in the Sylvania Inlier (Tyler, 1991) and overall the region has been interpreted as a fold-and-thrust-belt accompanying development of an inferred Ophthalmia mountain range (Fig. 3) (Powell et al., 1999). Extensional collapse of the Ophthalmia mountain range after the cessation of the Ophthalmian

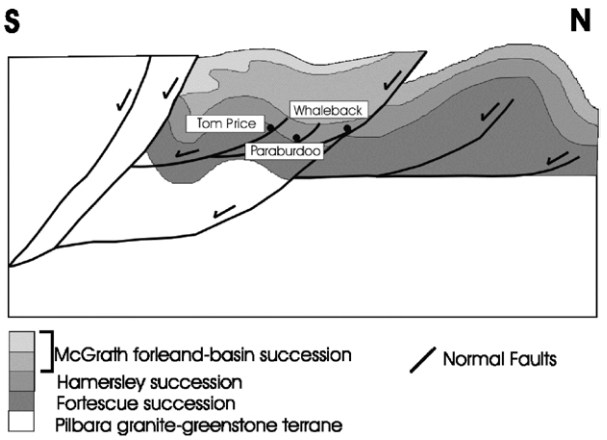

Fig. 3. Simplified regional geological cross-section and summary of stratigraphic groups (modified from Powell et al., 1999).

Orogeny at ca. 2200 Ma involved inversion of thrust faults (Powell et al., 1999), and development of new normal faults. Collectively these normal faults have been implicated as major fluid pathways resulting in ore genesis (Oliver and Dickens, 1999; Powell et al., 1999; Taylor et al., 2001) although absolute timing remains uncertain (2200 Ma versus ca. 2000 Ma). Later stage folding (F_3) informally known as 'Panhandle folding' along NW trends is best evidenced in the western part of the Hamersley Province (Taylor et al., 2001), although is not apparent around Mt Whaleback. A fourth compression (F_4) known as the Capricorn Orogeny was a significant ca. 1800 Ma event that resulted in W–NW-trending, open to upright folds, with up to kilometre scale wavelengths. These are most prominent in the north, central and western areas, and do not significantly affect our model scenarios.

2.2. Ore genesis models and fluid flow history

Proposed geological models for formation of giant microplaty hematite ores have varied throughout the last two decades, and most recently Taylor et al. (2001) have described a four stage process involving initial upward migration of deep seated basinal fluids followed by downward penetration of surficial fluids, resulting in multistage ore formation. The first hypogene stage involved upward migration of highly saline fluids through the Wittenoom Formation to the lower parts of the Brockman Iron Formation (Taylor et al., 2001). This stage of ore formation removed silica from the BIF units but preserved magnetite. The second stage resulted from the interaction of a moderately warm (ca. 100–200 °C) low salinity oxidising fluid, which converted magnetite–siderite to hematite–ankerite and developed microplaty hematite and martite in the process. A third stage of gangue removal stripped carbonates and silicates from these zones, and finally supergene weathering destroyed minor components such as apatite to complete the ore process. Other recent models include a syntectonic model involving possible fluid mixing

(Hagemann et al., 1999; Oliver and Dickens, 1999; Powell et al., 1999) and a deep hypogene model (Li et al., 1993). An early supergene model was proposed by Morris (1980, 1985), which involved electrically conductive BIFs as the main ingredient in a near surface electrochemical cell, although this model is now in question for the three microplaty hematite deposits (Taylor et al., 2001). Within all models two aspects of ore formation are commonly accepted: (1) ore genesis involved replacement of BIFs, and (2) ore bodies are spatially related to structural features, e.g. fault and folds. In the more recent models a broad similarity is present in that isotopic, fluid inclusion, geochemical and structural data suggest that both deep seated and surficial (meteoric) fluids were involved in ore genesis, and possible upward and downward penetration of fluids within an extensional environment were important. Thinning of BIF units, silica loss and porosity development accompanied geochemical transitions of BIF to ore (Webb et al., 2003). Ore formation proceeded primarily by silica loss (Taylor et al., 2001; Webb et al., 2003) with accompanying increase in porosity.

3. Theoretical background/mechanical modelling

3.1. Finite difference code

Models were developed by using the two-dimensional continuum code FLAC v.4.0 (Fast Lagrangian Analysis of Continua; Cundall and Board, 1988), which treats rock masses as continua represented by average values of mechanical and fluid flow properties. Materials are represented by a grid made up of elements or zones, which can be adjusted to fit the geometry to be modelled. Each element is assigned material properties such as bulk modulus, shear modulus and density, and elements deform according to a prescribed linear or non-linear stress/strain law in response to the applied forces or boundary conditions. FLAC uses an explicit time marching solution scheme and a form of dynamic relaxation. Because the solution is by numerical relaxation, and no matrices are formed, large two-dimensional calculations can be made with modest memory requirements. FLAC has the ability to model coupled deformation and fluid flow. Fluid flow obeys Darcy's Law and is considered to be compressible. FLAC-defined permeability and porosity represent initial conditions, although explicit rules governing permeability can be added. However, most of the hydrodynamic action in the models is a consequence of the change of volume affecting the hydraulic head, induced as a consequence of the deformation of dilatant rock materials.

3.2. Mechanical relationships

Applying a suitable constitutive model is the first step in any mechanical modelling study, and the classical Mohr–Coulomb material with non-associated plasticity is most suited to represent the rheology of the mid to upper crust (Vermeer and de Borst, 1984; Hobbs et al., 1990; Ord and Oliver, 1997). A Mohr–Coulomb material will deform elastically up to a yield point and then deform in a non-recoverable plastic manner (Ord and Oliver, 1997; Fig. 3). Failure will occur in a material if:

$$|\tau_s| = c - \sigma_n \tan\phi \tag{1}$$

where τ_s and σ_n are the shear and normal stresses across arbitrary planes within a material, and c and ϕ are material constants (cohesion and friction angle, respectively). During plastic deformation a Mohr–Coulomb material will shear, and this can be associated with dilation or a volume change. The microstructural processes involved have been highlighted by Vermeer and de Borst (1984), Ord and Oliver (1997), and more recently by Gow et al. (2002). During deformation rocks can compact and dilate, therefore dilation can be represented by both positive and negative values of strain:

$$\sin\psi = \epsilon_v^p / \gamma^p \tag{2}$$

where ψ is the dilation angle, ϵ_v^p is the rate of plastic volumetric strain, and γ^p is the rate of plastic shear strain. Local positive dilation is crucial in deforming porous media as it typically influences fluid flow direction more abruptly than the gentle gradients associated with topography or broadly distributed strains. For a more comprehensive explanation see Vermeer and de Borst (1984).

3.3. Fluid flow theory

The movement of crustal fluids occurs as a response to head gradients and buoyancy forces hydraulic head (H) is a measure of mechanical energy per unit weight of fluid, equivalent to the height above an arbitrary datum, e.g. sea level, to which fluid will rise in a well. The simplest form of equation describing hydraulic head is an elevation and pressure term:

$$H = z + P/\rho g \tag{3}$$

where H is the hydraulic head, z is the elevation above a datum, P is the pore fluid pressure, ρ is the density of the fluid, and g is the acceleration due to gravity. The governing equation determining fluid flow in a porous media can be expressed by Darcy's Law:

$$V_i = k_{ij} \frac{\gamma_f}{\eta_f} \left(\frac{\partial H}{\partial x_j} \right) \tag{4}$$

where V_i is the Darcy fluid velocity ($m\,s^{-1}$), k_{ij} is the permeability tensor (m^2), γ_f is the specific weight ($kg\,m^{-2}\,s^{-2}$), η_f is the viscosity ($kg\,m^{-1}\,s^{-1}$) of the fluid, H is the hydraulic head ($P/\rho g + z$) (m) and x_j is the position of a material point. Darcy's Law shows that differences in hydraulic head are required for flow to occur, and a static

homogenous rock package with topographic relief displays classical Darcian flow as a result of these head gradients. Darcy fluid flow vectors are by definition orthogonal to contours of hydraulic head in an isotropic medium with a constant density.

3.4. Deformation and fluid flow coupling

In a fluid saturated porous media that is deforming, effective stress is generally changing. Instantaneous changes in pore pressure (and hence effective stress) will result from local changes in total stress, but fluid flow is not instantaneous because it is governed by Darcy's Law. The fluid accommodates these changes in total stress, and the system responds by outward flow from regions of high or increased total stress, with the material deforming elastically and plastically as the fluid migrates away. In elastic and Mohr–Coulomb materials the constitutive relationships have no intrinsic time-dependence during such deformation. Our structural analysis relies on a 'poro-plasticity' model, and hence fluid will focus in areas of failure (at yield in shear or tension) within the model. Our models do not explicitly calculate the variation of porosity and permeability at each step during the model cycle. Rather, the material properties (including dilation angle), when subjected to stress, influence an 'elasto-plastic' volume change. This is related to and influenced by pore pressure at that point, and the implicit link to flow is via the pore pressure and hydraulic head (gravitational) parts of Darcy's Law. Thus, there is a 'pseudo'-porosity change at each step, which is manifest in the numerical calculations as a volume change (+ve or −ve dilation). This differs from models in which fluid pressure changes are purely a 'poro-elastic' response to applied stress. Effective stress is thus not an imposed variable, but one that is calculated for every step in every zone within the model during its cycle.

The emphasis of previous work (e.g. Ge and Garven, 1992) has been focused on the elastic part of stress–strain behaviour (the poro-elastic effect) and has concentrated on the generation of regions of high pore pressures due to elastic decrease in total volume by an imposed stress. This typically results in fluid being 'squeezed' out of the stressed regions. In contrast, in poro-plastic models high strain typically causes positive dilation of rocks and pore pressure decrease, and hence fluid is drawn in. Changes in volume due to plastic deformation are governed by the dilation angle of the rocks (ψ), and these changes in volume result in changes in pore pressure (Ord, 1991; Ord and Oliver, 1997). This effect on pore pressure is linked to changes in hydraulic head, which drives fluid flow, in accordance with Darcy's Law. Therefore, volume change is related to changes in effective stress, which can lead to further plastic deformation, which feeds back to more volume change. This feedback between deformation and fluid flow continues in a coupled manner.

4. Boundary conditions and model parameters

4.1. General conditions

Boundary conditions of the models are such that they represent upper-crustal conditions and are appropriate to deformation of an inverted sedimentary basin during inversion. Initial pore pressure gradients are equivalent to fully saturated hydrostatic conditions, with atmospheric pressure applied to the top of the model and 40 MPa at the base, consistent with the 4 km depth of the base of the mountain range and assuming homogeneous fluid density of 1000 kg/m^3. Later models incorporating basement material have a supra-hydrostatic starting pore pressure within such material. While rocks may not be saturated at depth, this assumption equates with the concept of fluid migration through networks of hydrofractures at scales finer than the grid zone dimensions (Ord and Oliver, 1997). Fluid pressure is specified in relation to depth and pressure at the base and sides of the model, at the start of the model runs; it subsequently wanes overall during extensional deformation. Each model is run and allowed to reach equilibrium under gravity before external deformation is applied. The models are subject to lateral extension and deformed to approximately 10% total strain. The base of the model is fixed vertically, but is free to extend in the horizontal direction. The sides of the model have a fixed horizontal velocity and remain planar, but are free to move in the vertical direction. The top surface is free to deform in any manner (Fig. 4). Material properties for all models discussed in this paper are listed in Table 1, which are representative of upper crustal materials and are in accordance with values proposed by previous authors (e.g. Ord and Oliver, 1997; Upton, 1998; Gow et al., 2002). Input parameters were varied during sensitivity testing, and variations included dilation angle (between 1 and 5°), permeability (2 orders of magnitude), cohesion, shear modulus, pore pressure (lithostatic–hydrostatic), bulk modulus and rates of deformation. Bulk modulus, dilation angle and deformation rates were the parameters least sensitive to change. In order to ensure that normal displacement occurred across the fault zone, cohesion and shear strength were specified at 2.00×10^2 and 3.00×10^7 Pa, respectively (Table 1) for the fault zone material, 2 to 4 orders of magnitude lower than the surrounding materials.

Simple conceptual models were devised to individually determine the effect of topography, extension and simple structures on fluid flow, and relate this to extensional collapse of mountain belts. The models are comprised of 120×60 grid zones and represent a section of upper crustal material initially 12 km wide and 3 km deep, with an additional topography 1 km high in the centre of the model (corresponding to a mountain range). Four basic variations (Models 1–4) (Fig. 5) are: (1) mountain range without deformation, (2) mountain range undergoing extension, (3) mountain range extension with a permeable shear zone

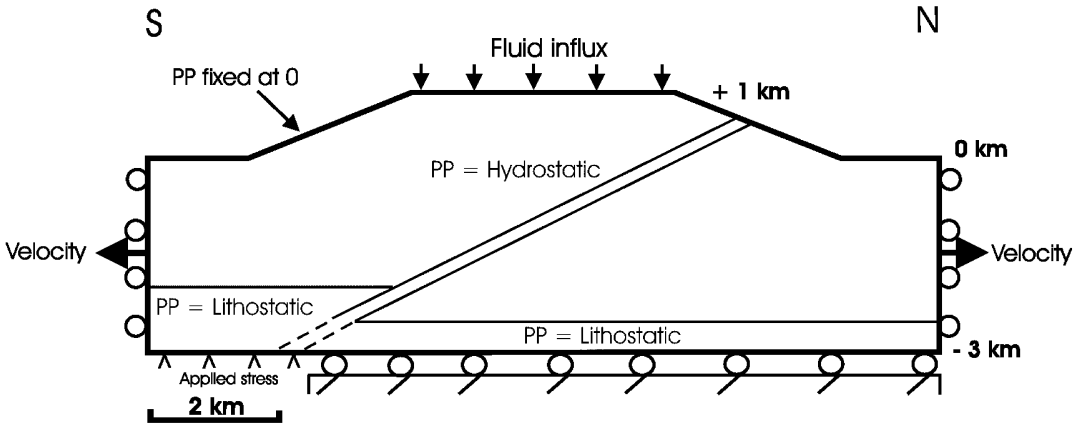

Fig. 4. Mechanical boundary conditions for all models. The geometry is progressively altered throughout the models but basic conditions remain constant. Rolling boundaries allow extension or contraction but edges remain planar. Initial pore pressure conditions are hydrostatic but were allowed to change on all boundaries during deformation. A stress equal to the overburden is applied at the base of the hanging wall, which allows normal sense movement on the fault during extension but prevents the base of the model from collapsing. Pore pressure is fixed at zero at the top of the model, hydrostatic initially in most of the models throughout the mountain range, and lithostatic initially at the base of some models. Fluid is applied to the top of the model at a rate of 1×10^{-10} m s^{-1} simulating rainfall.

(inverted thrusts), and (4) effect of low permeability basement material.

4.2. Hamersley specific models

Based especially on the Hamersley Province, Model 5 consists of a 12 km × 3 km two-dimensional block of upper crustal material with additional 1 km of topographic relief (as per Model 1), which represents simplified topographical and geological elements of an inferred mountain range. Additional structures were progressively added to the basic model, including a fault (Model 3), granite basement blocks (Model 4) and stratigraphy (Model 5) (Fig. 6). This staged process allowed verification of model parameters and sensitivity testing as the modelling progressed. The constitutive model and boundary conditions are as for earlier models (1–4), with the basement pore pressure initially set as lithostatic.

Model 6 examines the effect of increasing permeability of BIF units, as a proxy for silica dissolution, but could equally well be applied to carbonate dissolution in other environments. The conceptual model is that of Model 5 and model parameters include a variation of permeability considerations with a range from 2.00×10^{-16} to 1.00×10^{-13} m^2 (appropriate to porous and fractured rock), with permeabilities within layered BIF units being allowed to change as a function of fluid flux, through use of an internal macro language (FISH). Six variations of this additional function were applied to the model as a first step in attempting to simulate reaction-enhanced permeability in the BIF layering. As fluid flow within the BIF layers reaches a predefined threshold, permeability is allowed to change incrementally (Fig. 7). A limit on permeability increase was introduced to represent the possibility of compaction, which would inhibit very high porosities (due to overburden load). The mineralogy of the BIF sequences consists of approximately 50% quartz and 50% iron oxide, so an upper porosity limit of the BIFs would therefore be around 50%,

Table 1
Material properties for numerical models

Model	Density (kg/m^3)	Bulk modulus (Pa)	Shear modulus (Pa)	Friction angle (°)	Cohesion (Pa)	Dilation angle (°)	Permeability (m^2)
Models 1–5(Mohr–Coulomb)							
Upper Crust	2700	2.33×10^{10}	6.4×10^{9}	30	1.0×10^{7}	3	1.0×10^{-15}
Fault	2400	2.33×10^{8}	3.0×10^{7}	30	2.0×10^{2}	4	1.0×10^{-13}
Granite	2650	4.95×10^{10}	2.9×10^{10}	30	4.0×10^{6}	3	2.0×10^{-16}
BIF	2400	3.2×10^{10}	4.0×10^{9}	30	3.0×10^{6}	4	1.0×10^{-14}
Shale	2500	2.81×10^{10}	6.69×10^{9}	30	3.0×10^{6}	4	1.0×10^{-19}
Model 6 (Mohr–Coulomb)							
Upper Crust	2700	2.33×10^{10}	6.4×10^{9}	30	1.0×10^{7}	3	1.0×10^{-15}
Fault	2400	2.33×10^{8}	3.0×10^{7}	30	2.0×10^{2}	4	1.0×10^{-13}
Granite	2650	4.95×10^{10}	2.9×10^{10}	30	4.0×10^{6}	3	2.0×10^{-16}
BIF[a]	2400	3.2×10^{10}	4.0×10^{9}	30	3.0×10^{6}	4	1.0×10^{-14} to 1.0×10^{-12}
Shale	2500	2.81×10^{10}	6.69×10^{9}	30	3.0×10^{6}	4	1.0×10^{-19}

[a] Reaction enhanced permeability function applied.

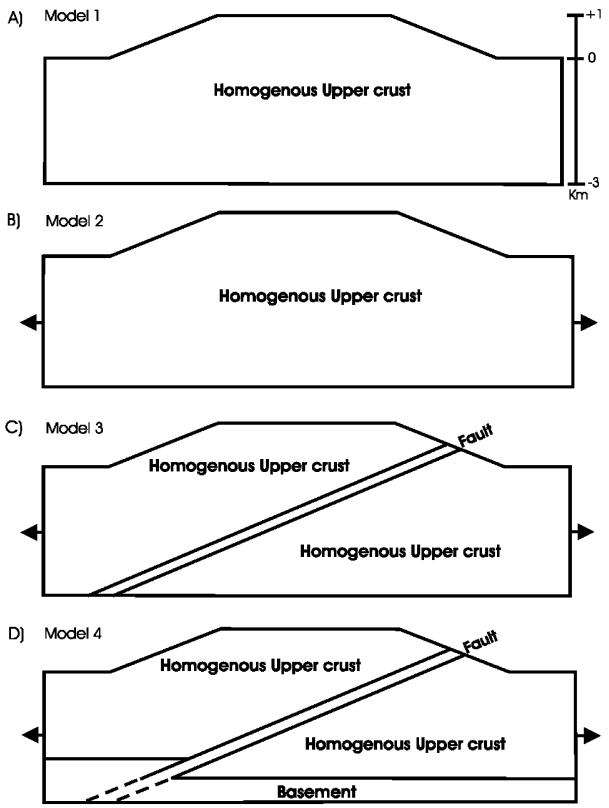

Fig. 5. Starting conditions for four basic conceptual models (1) mountain range without deformation, (2) mountain range undergoing extension, (3) normal sense reactivation of former thrust faults, and (4) basement impermeable block and collapse of basement thrust. Note: vertical scale = horizontal scale.

irrespective of compaction. Compaction of these units would decrease the overall porosity and actual ores show an average porosity of around 25% (Webb et al., 2003). Sensitivity analysis was used to constrain possible variations of BIF permeability as a function of fluid flux rates (Fig. 8A and B). As a result of the sensitivity analysis and the previous discussion on maximum porosity values of the BIF the reaction enhanced code 02 was used in Model 6, which allowed the BIF units to become 1 order of magnitude more permeable than the fault.

5. Model results

5.1. Static mountain range (Model 1)

The model of a non-deforming mountain range displays classic Darcian flow, where topographic flow is driven by hydraulic head gradients in a 'fan-shaped' pattern, with flow generally orthogonal to head gradients (Fig. 9). This is in accordance with the typical profile envisaged by hydrologists as previously shown by Hubbert (1940) and Tóth (1962, 1963), and is also consistent with the idea that topographic relief is responsible for much groundwater flow in continental landmasses (Hubbert, 1940; Garven and Raffensperger, 1997).

5.2. Mountain range extension (Model 2)

During extensional deformation fluid flow is focused towards areas of dilation and is concentrated towards the centre of the mountain range, although topographically driven gradients still have some influence over fluid flow Pore pressure within the range decreases rapidly with time as a result of deformation, which drives fluid flow into the centre and base of the model where the decrease in pore pressure is most notable (Fig. 10). Variations in rates of deformation were tested and the major flow pattern within the models still displayed downward migration of fluids, albeit less prominently in slowly deforming systems. Collapse of strongly inverted basins or mountainous fold-and-thrust-belts during extensional deformation has a major effect on fluid flow, relative to the 'fan-shaped' topographically driven flow as shown within a static mountain range.

5.3. Mountain range extension with shear zone (Model 3)

Addition of a structure such as a permeable fault or shear zone has a major influence on the fluid flow within a collapsing mountain range. In continuum codes such as FLAC, such zones must have a finite width, and have been set at two zones wide (= 200 m). Limitations on the geometry construction prevent using narrower fault zones for adequate display purposes. The addition of a permeable

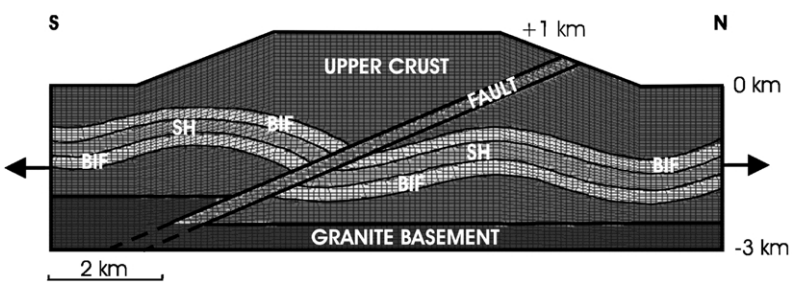

Fig. 6. Conceptual Model 5 consists of a 12 km × 3 km two-dimensional block of upper crustal material with additional 1 km of topographic relief, which represents simplified topographical and geological elements of an inferred Opthalmian mountain range. Additional structures include a fault, a granite basement block, and folded stratigraphy (BIF—banded iron formation, SH—shale).

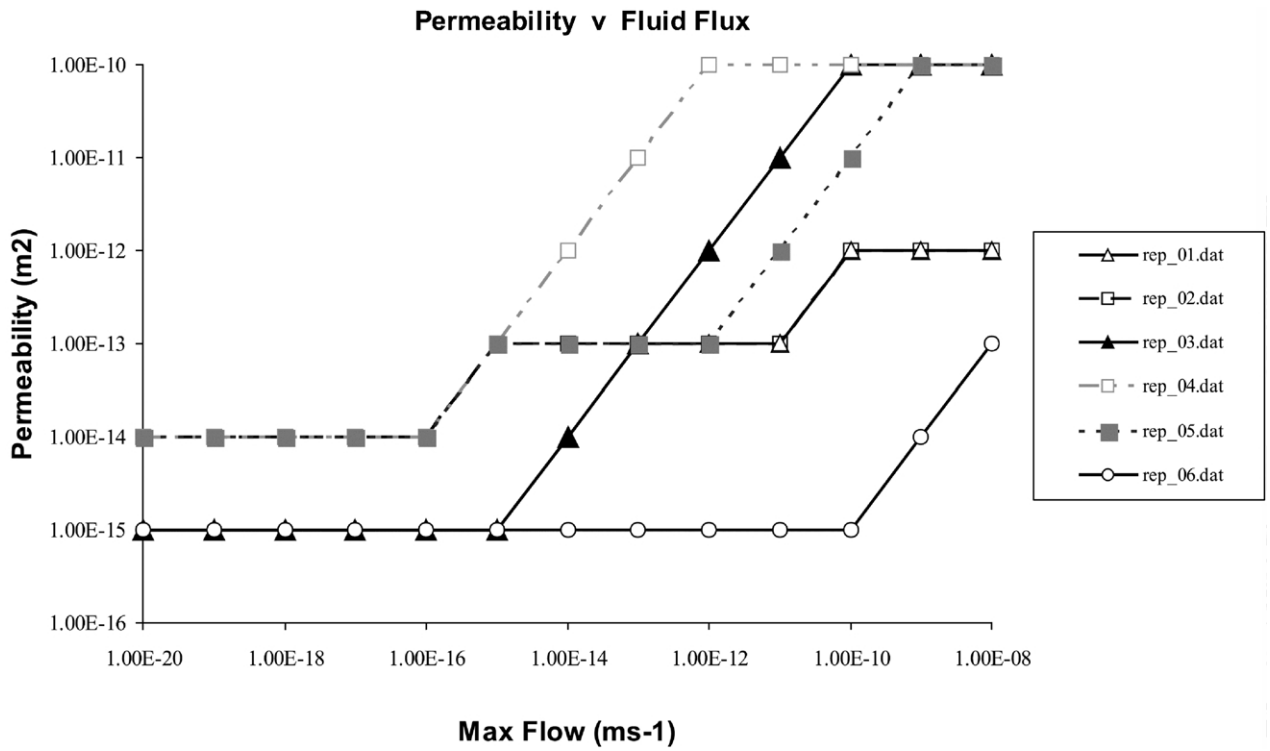

Fig. 7. Six variations of the reaction enhanced permeability function applied using FISH code. This function is applied to BIF layering only. As fluid flow within the BIF layers reaches certain levels, permeability is consequently allowed to change. The plateaux were introduced to represent the potential for compaction, hence a reduction or temporary stasis in permeability within the BIFs. This stasis also provides a limit on permeability creation equivalent to the total amount of silica in original BIF (ca. 50%). Maximum variation in permeability is 1.00×10^{-15} to 1.00×10^{-10} m^2.

fault provides a primary fluid pathway and fluid is focused into and along the fault zone. High permeability and dilation within the fault allows the downward migration of surficial fluids, which is driven by topography and hydraulic head gradients. Pore pressure gradients and the evolution of pore pressure due to deformation (Fig. 11A) drives upward flow from the base of the fault, as local areas of contraction and high shear strain expel fluids. These areas of fluid expulsion are associated with low hydraulic head and negative volumetric strain (Fig. 11B). There is competition between upward and downward flow through time, so as the model progresses and extension matures, downward flow becomes more prominent due to a decrease in hydraulic head and an overall decrease in pore pressure throughout the model with

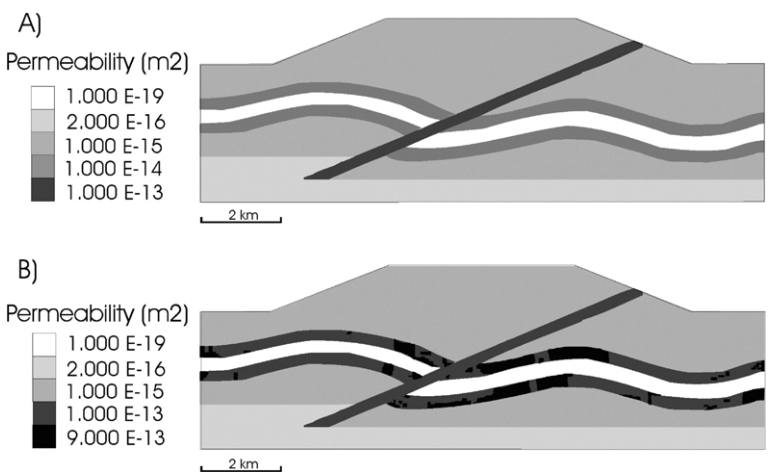

Fig. 8. Two stages of the permeability change in BIF layers. Contours represent values of permeability (darkest colours represent highest permeability). (A) Starting conditions of permeability, (B) permeability increasing along BIF layers to greater than that of the fault. Additional code (rep_02) was used in this model (see Fig. 7).

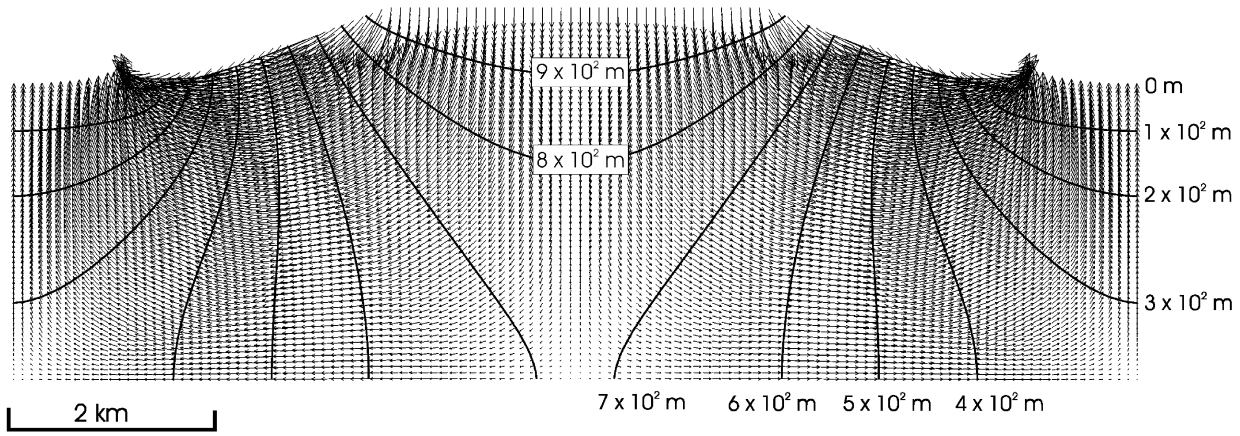

Fig. 9. Model 1 with topography but no deformation displaying classic Darcian flow and hydraulic head contours, where topographic flow is driven by head gradients in a 'fan-shaped' pattern (e.g. Tóth, 1962, 1963). Flow is generally orthogonal to hydraulic head gradients. Arrows indicate Darcy flow vectors, maximum vector is 1.45×10^{-3} m yr^{-1}. Conservative flow time is 2.06×10^{5} yrs.

time. Topographic driven flow utilises the least restrictive pathway of the fault and this is in competition with pressure-driven flow from near the base of the model.

5.4. Low permeability basement (Model 4)

Granite blocks were introduced into the model to simulate both basement and overthrust basement blocks. We assume that the granite has a low permeability and that pore pressure near the bottom of sedimentary basins increases due to porosity reduction with depth. The elevated pore pressure and low permeability has the effect of driving fluid from the basement rocks, and these fluids are focused within the more permeable fault zone (Fig. 12A). The effects of an overpressurised basement forces fluids upwards within the fault, which provides a greater resistance to downward migrating fluids than seen in previous models. As observed in Model 3, there is strong competition between upward and downward migration of fluids within the fault zone. As extension continues, pore pressure within the model begins to decrease and this allows surficial fluids to penetrate deeper into the model. Even with the added basement blocks and elevated pore pressures in the initial stages of these models, fluids penetrating from the surface overcome this and dominate the overall direction of fluid flow within the model as deformation continues and pore pressures decrease (Fig. 12B).

5.5. Application to the Hamersley Province (Model 5)

One of the most important results from these numerical models is the simulation of upward and downward migration of fluids during extension. At early stages of deformation, upward flow from the base of the model is apparent (Fig. 13A) and this can be attributed to variations in pore pressure, hydraulic head and volumetric changes due to deformation as discussed for previous models. The introduction of stratigraphic layering allows lateral fluid flow within the model and fluids enter the BIF units from the more permeable fault where areas of potential fluid mixing are noted at the fault and BIF boundaries (Fig. 13B). Displacement within the model shows normal sense movement around the fault consistent with extensional deformation and reactivation of previous thrust faults. As extension progresses, upward flow becomes less prominent, and downward migration of fluids is attributed

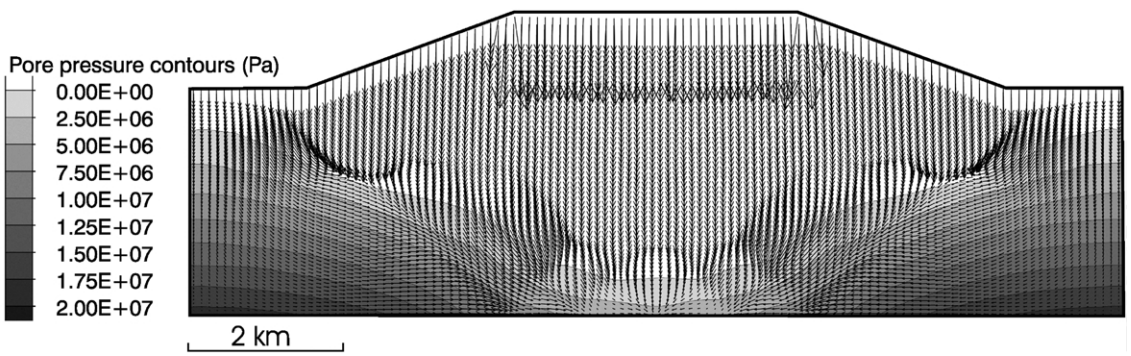

Fig. 10. Model 2 at 3% deformation. Pore pressure decrease is noted in the centre and base of the model, which is driving fluid flow towards these areas. As a result of extension fluid is focused towards dilational areas and into the centre of the mountain range. Arrows indicate Darcy flow vectors, maximum vector is 1.01×10^{-2} m yr^{-1}.

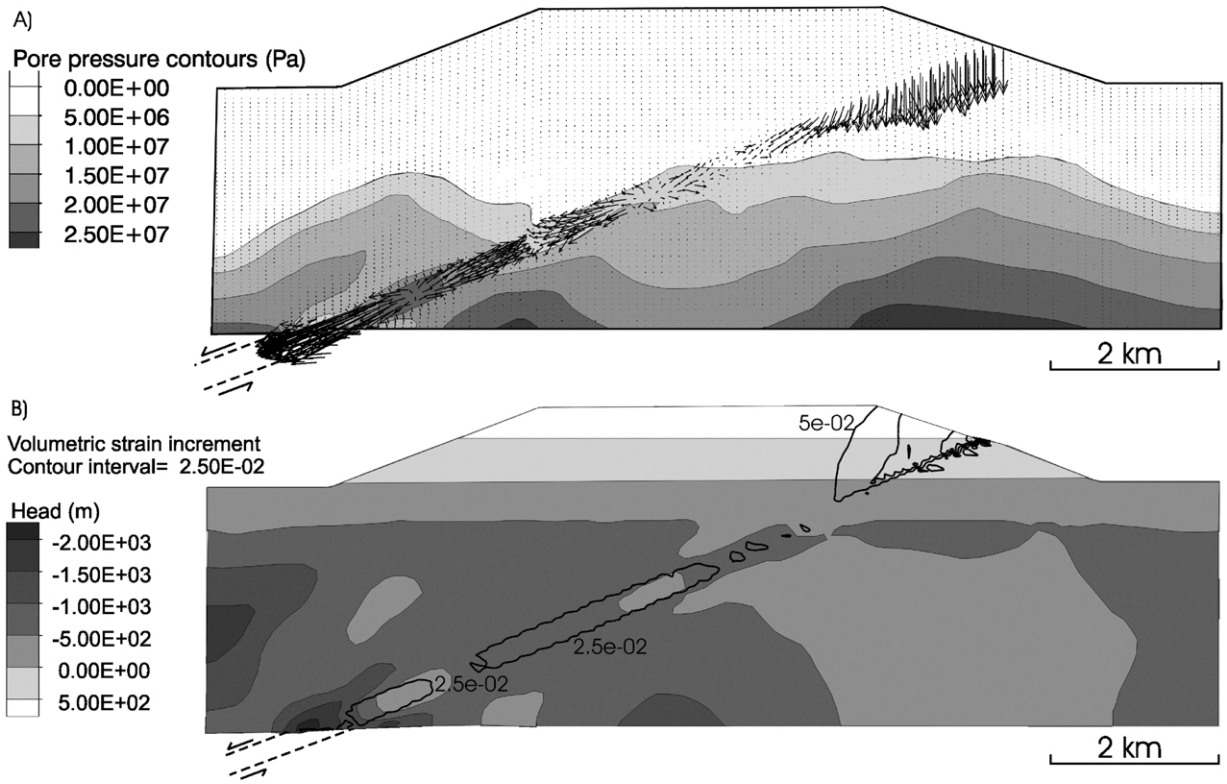

Fig. 11. Model 3 at 3% deformation. (A) Pore pressure variations showing an overall pore pressure decay displayed within the model with areas of increased pore pressure evident within the fault zone, which is forcing fluids from these areas, and (B) volumetric strain increment contours and hydraulic head showing low values within contractional areas of the fault zone corresponding to fluid expulsion. Arrows indicate Darcy flow vectors, maximum vector is 7.6×10^{-1} m yr^{-1}.

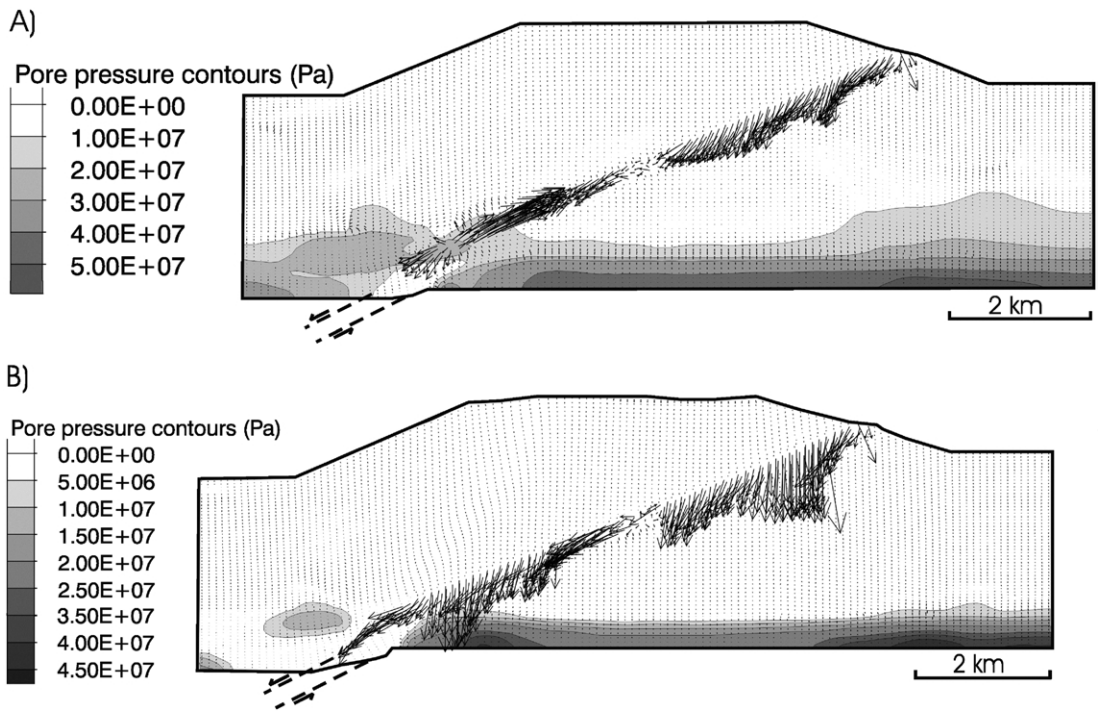

Fig. 12. Model 4 (A) at 3% deformation, displaying reducing pore pressures within the model as extension progresses, and showing upward and downward fluid flow within the fault zone (arrows indicate Darcy flow vectors, maximum vector is 3.9×10^{-1} m yr^{-1}) and (B) at 7% deformation, displaying further pore pressure reduction and downward prominent flow, as surficial fluids compete with deep seated fluids (arrows indicate Darcy flow vectors, maximum vector is 4.01×10^{-1} m yr^{-1}).

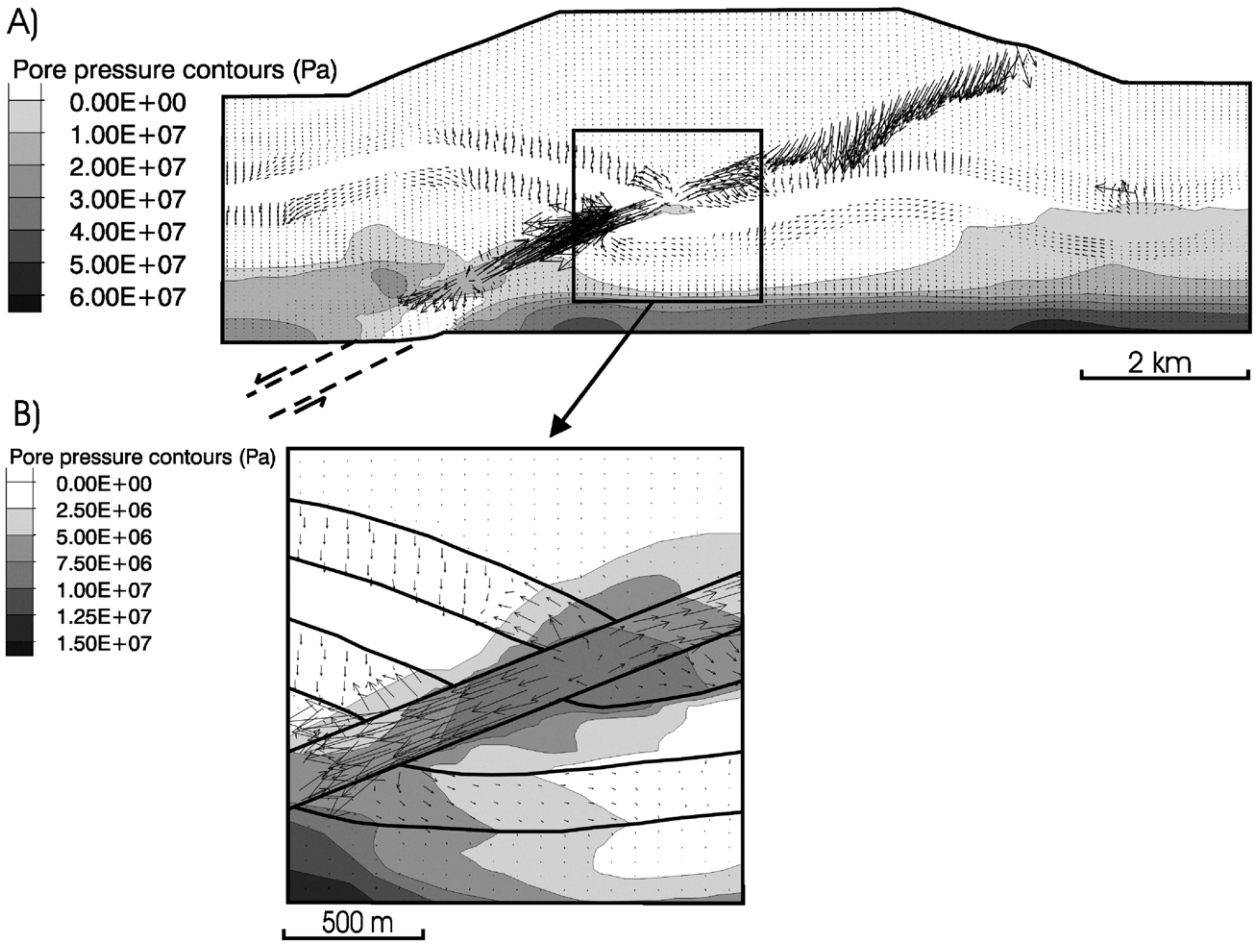

Fig. 13. Model 5 at 3% deformation (A) displaying pore pressure reduction with upward and downward migration of fluids and lateral flow within the BIF layers. Areas of high pore pressure within the fault expel fluids, arrows indicate Darcy flow vectors, maximum vector is 4.97×10^{-1} m yr^{-1}. (B) Pore pressure values and flow vectors are highlighting areas of fluid mixing within the BIF layers.

to deformation induced flow and decrease in pore pressure (Fig. 14A). Failure modes within the model (Fig. 14B) demonstrate that tensile yield is predominantly seen at shallow depths, shear failure is prominent at depth and along the fault zones. Zones indicated as 'elastic, at yield in past' represent areas where pore pressure has dropped such that the rocks have moved off the tensile or shear failure conditions. These areas sweep through the model as fluid is channelled towards the fault, and are most prominent in the fault's hanging wall.

5.6. Silica dissolution of BIFs (Model 6)

When the reaction enhanced permeability function is applied to the BIF layering in the model, lateral fluid flow is increased along the BIF layers (Fig 15A). Fluid migrates from within the fault zone and enters the BIF layers indicating a high potential for fluid mixing close to the fault and BIF interface (Fig. 15B). Fluid flow within the BIF units approaches and exceeds that of the faults due to the dissolution of silica and changes in porosity (up to 50%). As the model progresses again downward fluid flow becomes more prominent within the fault zone (Fig. 16).

6. Discussion and conclusions

Mechanical and geological conditions appropriate to both upward and downward migration of fluids within a mountain range have been explored within these models. The presence of topography in a basic model demonstrates the strong influence of hydraulic head and topographic driven flow in any homogenous package of rock. However, the effect of extension drives fluid flow into the centre of the model, and even for low strain rates this strongly modifies the flow pattern away from the simple curved topography-only pattern. This effect on fluid flow is due to the focusing of fluid to areas of predicted shear and extensional failure and driven by pore pressure gradients within the model. This competes with the strong effect of topographic driven flow during the early stages of mountain collapse. The addition of a permeable normal fault (Model 3), causes perturbations to this downward focusing, as the permeability contrasts

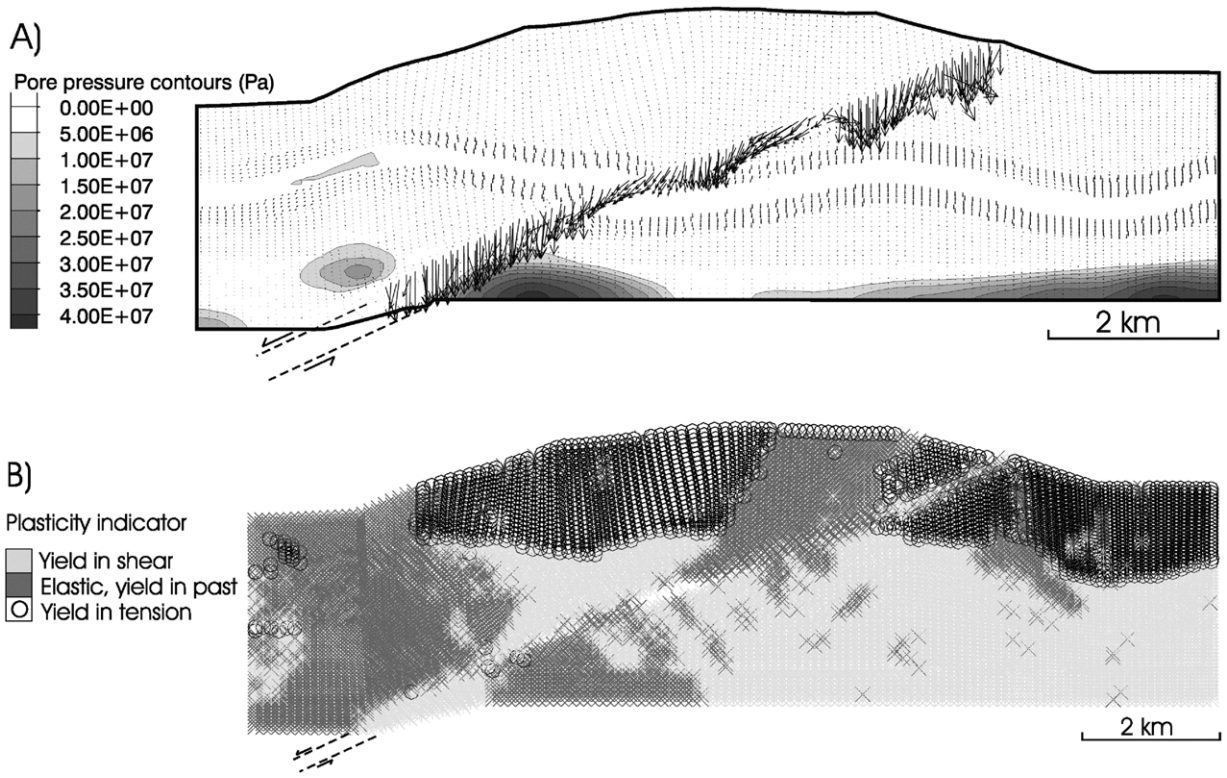

Fig. 14. Model 5 at 10% deformation (A) displaying reduced pore pressure within the model due to failure and extension. Downward fluid flow is prominent, with lateral flow within the BIF layers. Arrows indicate Darcy flow vectors, maximum vector is 4.97×10^{-1} m yr^{-1}. (B) Plasticity indicator or state of failure of the model, indicating different types of failure within the model. Tensile failure is predominantly shown in the upper half of the model.

between the fault and the surrounding rock enables focusing of fluids within the more highly permeable fault. The more permeable fault represents the least restrictive fluid pathway and fluids are drawn from the surrounding package of porous rock into the fault and result in a focused downward migration of surficial fluids. This flow competes with the upward migration of fluids seen at the base of the models due to deformation and overpressurisation.

During extension there is failure and dilation of the rocks, which focuses flow, and a gradual reduction in pore pressure and hydraulic head gradients as the mountain collapses. As pore pressures drop within the mountain range upward migration of fluids becomes less prominent and downward flow more prominent. The introduction of a granitic basement promotes upward flow due to simulated overpressure commensurate with low basement permeability and compaction related overpressure at the base of the sedimentary sequence. At early stages of extension, deformation-induced flow is evident in the lower parts of the fault, where contraction within the fault zone expels fluid, which coincides with areas of low hydraulic head and negative dilation. However, as the deformation continues and pore pressure decreases overall there is prominent downward penetration of surficial fluids within the fault.

This competing process of upward and downward migration of fluids has major implications for the genesis of the Hamersley iron ores. Ore genesis models of Taylor et al. (2001), Hagemann et al. (1999), Oliver and Dickens (1999) and Powell et al. (1999) are broadly similar in that they have proposed the involvement of both deep seated and surficial (meteoric) fluids. Upward migration of reducing alkaline fluids may have been responsible for the first stage of ore genesis by removing silica, and increasing porosity without altering the oxidation state of the iron-rich minerals. This stage has been proposed for the Tom Price deposit (Taylor et al., 2001), with a reduction of silica volume and no oxidation of magnetite to hematite. The second stage of ore genesis involved downward migration of surficial fluids that have converted magnetite–siderite to hematite–ankerite assemblages, developing the characteristic microplaty hematite and martite. Taylor et al. (2001) have proposed a third stage following oxidation, which removed all carbonate from hematite- and magnetite-rich zones and a final deep supergene stage that converted magnesium silicates to a kaolinitic residue. These last two stages would require prominent downward migration of oxidising fluids during the later stages of extension, which is supported by this modelling. At Mt Whaleback, where Webb et al. (2003) have not been able to distinguish separate silica loss and oxidation events, the process of downward flow of oxidised fluids may have been more complete than at Tom Price. In relation to our models, the difference could be due to the position of these deposits relative to upward and downward flow paths.

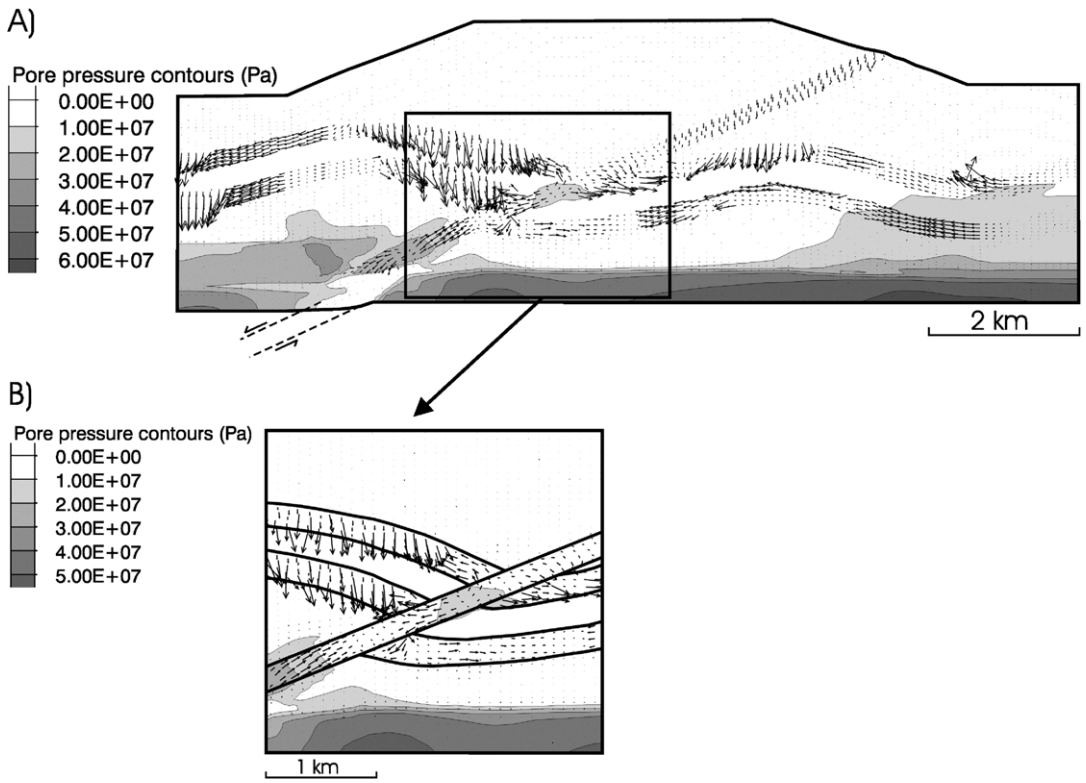

Fig. 15. Model 6 at 3% deformation using (rep_02) permeability function (A) displaying pore pressure values with upward and downward flow within the fault. Notable expulsion of fluid occurs within areas of high pore pressure due to deformation. Lateral flow within the BIF layers is much increased from previous models. Arrows indicate Darcy flow vectors, maximum vector is 2.44 m yr^{-1}. (B) Displaying pore pressure values with fluid migrating from the fault zone into the BIF layers, highlighting potential fluid mixing areas.

Stratigraphic layering within the mountain range allows lateral fluid migration towards the more permeable fault. Our models predict locations within BIF layers where actual mixing would occur, but also the gradual change from deeper seated fluid moving upwards to surface fluid moving downwards. In these models fluid mixing occurs at the stratigraphic and fault boundaries, and zones of fluid mixing penetrate into the BIF layers. In relation to iron ore genesis, this may represent mixing of deep basinal derived fluids and heated meteoric fluids in accordance with models of Oliver and Dickens (1999) and Powell et al. (1999). Fluid flow rates within these models are comparable with many other studies (Dipple and Ferry, 1992; Upton et al., 1995, 1998; Ord and Oliver, 1997; Upton, 1998; Oliver et al., 1999), and the introduction of the reaction-enhanced permeability allows flux rates to increase by one order of magnitude.

Allowing the permeability of BIF layers to increase as reducing fluids strip silica allows the model system to maintain lateral fluid migration, and is a key aspect of mineralisation. This dissolution of silica provided secondary fluid pathways along stratigraphic layering, which then allowed layer-parallel movement of heated meteoric oxidising fluids culminating in ore genesis. The potential fluid mixing areas within the BIF and close to the fault

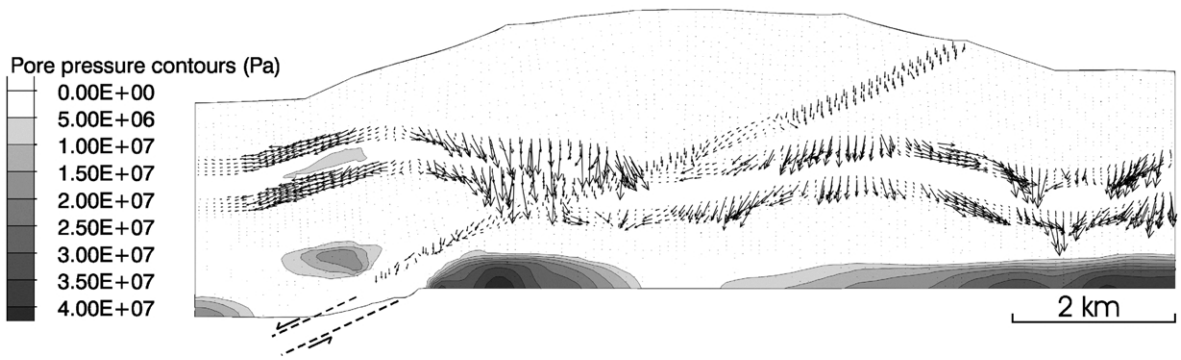

Fig. 16. Model 6 at 10% deformation. Pore pressure values decrease more rapidly throughout the model relative to Fig. 15 and downward fluid flow within the fault is dominant. Strong lateral flow is evident within the BIF layers. Arrows indicate Darcy flow vectors, maximum vector is 2.43 m yr^{-1}.

boundary within these models are the interpreted location for ore genesis as they provide conditions conducive for dissolution of silica and oxidation of magnetite to hematite in a two-stage process. Basement penetrating faults provide highly permeable fluid pathways to draw deep-seated fluids into the system to accommodate dissolution of silica, and connectivity of these pathways to the surface allows passage of surficial fluids to depths of 3 km or greater. Permeable faults, reaction enhanced permeability and lateral fluid migration have played a vital role in the genesis of giant Hamersley iron ores.

Acknowledgements

We would like to thank staff at the CSIRO EM, Jeff Loughran, Adam Webb and Matthew Brown (James Cook University) for comments and advice. We would also like to thank Chris Hanley and Peter Croft from BHP Billiton for logistical support. An ARC Large Grant to Oliver and Dickens also supported this study. Published with permission of Geo CEO, predictive mineral discovery crc.

References

Bethke, C.M., 1985. A numerical model of compaction-driven groundwater flow and heat transfer and its application to the paleohydrology of intracratonic sedimentary basins. Journal of Geophysical Research 90b, 6817–6828.

Bredehoeft, J.D., Hanshaw, B.B., 1968. On the maintenance of anomalous fluid pressures: I. Thick sedimentary sequences. Geological Society of America Bulletin 79, 1097–1106.

Brown, M.C., Oliver, N.H.S., Dickens, G.R., 2004. The characterization and paragenesis of veining and fluid flow in the Mt. Whaleback iron ore district, eastern Hamersley Province, Western Australia. Precambrian Research, in press.

Cox, S.F., 1999. Deformation controls on the dynamics of fluid flow in mesothermal gold systems. In: McCaffery, K.J.W., Lonergan, L., Wilkinson, J.J. (Eds.), Fractures, Fluid Flow and Mineralization. Geological Society Special Publication 155, pp. 123–140.

Cundall, P., Board, M., 1988. A microcomputer program for modelling large-strain plasticity problems. In: Swoboda, C., (Ed.), Numerical Methods in Geomechanics. Proceedings of the 16th International Conference on Numerical Methods in Geomechanics, pp. 2101–2108.

Dipple, G.M., Ferry, J.M., 1992. Metasomatism and fluid flow in ductile fault zones. Contributions to Mineralogy and Petrology 112 (2-3), 149–164.

Domenico, P.A., Schwartz, F.W., 1997. Physical and Chemical Hydrogeology, 2nd ed, John Wiley and Sons, New York.

Etheridge, M.A., Wall, V.J., Vernon, R.H., 1983. The role of the fluid phase during regional metamorphism and deformation. Journal of Metamorphic Geology 1, 205–226.

Etheridge, M.A., Wall, V.J., Cox, S.F., 1984. High fluid pressure during regional metamorphism and deformation: implications for mass transport and deformation mechanisms. Journal of Geophysical Research 89, 4344–4358.

Freeze, R.A., Witherspoon, P.A., 1966. Theoretical analysis of regional groundwater flow: 1. Analytical and numerical solutions to the mathematical model. Water Resources Research 2 (4), 641–656.

Garven, G., 1985. The role of regional fluid flow in the genesis of the Pine Point deposit, Western Canada sedimentary basin. Economic Geology 80, 307–324.

Garven, G., Freeze, R.A., 1984a. Theoretical analysis of the role of groundwater flow in the genesis of stratabound ore deposits. 1. Mathematical and numerical model. American Journal of Science 284, 1085–1124.

Garven, G., Freeze, R.A., 1984b. Theoretical analysis of the role of groundwater flow in the genesis of stratabound ore deposits. 1. Quantitative results. American Journal of Science 284, 1125–1174.

Garven, G., Raffensperger, J.P., 1997. Hydrogeology and geochemistry of ore genesis in sedimentary basins. In: Barnes, H.L., (Ed.), Geochemistry of Hydrothermal Ore Deposits, pp. 125–189.

Ge, S., Garven, G., 1992. Hydromechanical modelling of tectonically driven groundwater flow with application to the Arkoma foreland basin. Journal of Geophysical Research 97, 9119–9144.

Gow, P.A., Upton, P., Zhao, C., Hill, K.C., 2002. Copper–gold mineralisation in New Guinea: numerical modelling of collision, fluid flow and intrusion-related hydrothermal systems. Australian Journal of Earth Sciences 49, 753–771.

Hagemann, S.G., Barley, M.E., Folkert, S.L., Yardley, B.W., Banks, D.A., 1999. A hydrothermal origin for the giant Tom Price iron ore deposit. In: Stanley, C.J., et al. (Eds.), Mineral Deposits: Processes to Processing Balkema, Rotterdam, pp. 41–44.

Harmsworth, R.A., Kneeshaw, M., Morris, R.C., Robinson, C.J., Shrivastava, P.K., 1990. BIF-derived iron ores of the Hamersley Province. In: Hughes, F.E. (Ed.), Geology of the Mineral Deposits of Australia and Papua New Guinea. Australasian Institute of Mining and Metallurgy Monograph 14, pp. 617–642.

Hobbs, B.E., Muhlhaus, H.B., Ord, A., 1990. Instability, softening and localization of deformation. In: Knipe, R.J., Rutter, E.H. (Eds.), Deformation Mechanisms, Rheology and Tectonics, Geological Society Special Publication, pp. 143–165.

Hubbert, M.K., 1940. The theory of ground-water motion. Part 1. The Journal of Geology 48 (8), 785–944.

Kendrick, M.A., Burgess, R., Patrick, R.A.D., Turner, G., 2002a. Hydrothermal fluid origins in a fluorite-rich Mississippi Valley-type district: combined noble gas (He, Ar, Kr) and halogen (Cl, Br, I) analysis of fluid inclusions from the South Pennine ore field, UK. Economic Geology 97, 435–453.

Kendrick, M.A., Burgess, R., Leach, D., Patrick, R.A.D., 2002b. Hydrothermal fluid origins in Mississippi Valley-type ore districts: combined noble gas (He, Ar, Kr) and halogen (Cl, Br, I) analysis of fluid inclusions from the Illinois–Kentucky fluorspar district, viburnum trend, and tri-state districts, midcontinent, US. Economic Geology 97, 453–471.

Kissen, I.G., 1978. The principal distinctive features of the hydrodynamic regime of intensive earth crust downwarping areas. In: Ronai, A., Remi, M. (Eds.), Hydrogeology of Great Sedimentary Basins, Publication of the International Association of Hydrological Sciences, pp. 178–185.

Koons, P.O., Craw, D., Cox, S.C., Upton, P., Templeton, A.S., Chamberlain, C.P., 1998. Fluid flow during active oblique convergence: a Southern Alps model from mechanical and geochemical observations. Geology 26, 159–162.

Li, Z.X., Powell, C.McA., Bowman, R., 1993. Timing and genesis of Hamersley iron-ore deposits. Exploration Geophysics 24, 631–636.

Martin, D.M., Li, Z.X., Nemchin, A.A., Powell, C.M., 1998. A pre-2.2 Ga age for giant hematite ores of the Hamersley Province, Australia. Economic Geology 93, 1084–1090.

Morris, R.C., 1980. A textural and mineralogical study of the relationship of iron ore to banded iron formation in the Hamersley Iron Province of Western Australia. Economic Geology 75, 185–209.

Morris, R.C., 1985. Genesis of iron ore in banded iron-formation by supergene and supergene-metamorphic processes—a conceptual model. In: Wolff, K.H. (Ed.), Handbook of Strata-bound and Stratiform Ore Deposits 13, pp. 73–235.

Nesbitt, B.E., Muehlenbachs, K., 1989. Origins and movement of fluids

during deformation and metamorphism in the Canadian Cordillera. Science 245, 733–736.

Neuzil, C.E., 1995. Abnormal pressures as hydrodynamic phenomena. American Journal of Science 295, 742–786.

Oliver, J., 1986. Fluids expelled tectonically from orogenic belts: their role in hydrocarbon migration and other geologic phenomena. Geology 14, 99–102.

Oliver, N.H.S., 1996. Review and classification of structural controls on fluid flow during regional metamorphism. Journal of Metamorphic Geology 14, 477–492.

Oliver, N.H.S., Dickens, G.R., 1999. Hematite ores of Australia formed by syntectonic heated meteoric fluids. In: Stanley, C.J., et al. (Eds.), Mineral Deposits: Processes to Processing Balkema, Rotterdam, pp. 889–892.

Oliver, N.H.S., Pearson, P.J., Holcombe, R.J., Ord, A., 1999. Mary Kathleen metamorphic–hydrothermal uranium–rare-earth element deposit: ore genesis and numerical model of coupled deformation and fluid flow. Australian Journal of Earth Sciences 46, 467–484.

Oliver, N.H.S., Ord, A., Valenta, R.K., Upton, P., 2001. Deformation, fluid flow, and ore genesis in heterogeneous rocks, with examples and numerical models from the Mount Isa District, Australia. Society of Economic Geologists, Reviews 14, 51–74.

Ord, A., 1991. Deformation of rock: a pressure-sensitive, dilatant material. Pure and Applied Geophysics 137 (4), 337–366.

Ord, A., Oliver, N.H.S., 1997. Mechanical controls on fluid flow during regional metamorphism: some numerical models. Journal Metamorphic Geology 15, 345–359.

Ord, A., Hobbs, B.E., Zhang, Y., Broadbent, G.C., Brown, M., Willetts, G., Sorjonen-Ward, P., Walshe, J.L., Zhao, C., 2002. Geodynamic modelling of the Century deposit, Mt Isa Province, Queensland. Australian Journal of Earth Sciences 49 (6), 1011–1039.

Powell, C.McA., Li, Z.X., Martin, D.McB., 1998. Tectonic evolution of the Paleoproterozoic Ophthalmia fold and thrust belt. 14th Australian Geological Convention [abs.], Geological Society of Australia, 361pp.

Powell, C.McA., Oliver, N.H.S., Li, Z.X., Martin, D.McB., Ronaszeki, J., 1999. Synorogenic hydrothermal origin for giant Hamersley iron oxide. Geology 27, 175–178.

Schaubs, P.M., Zhao, C., 2002. Numerical models of gold-deposit formation in the Bendigo–Ballarat Zone, Victoria. Australian Journal of Earth Sciences 49 (6), 1077–1096.

Sharpe, R., Gemmell, J.B., 2002. The Archean Cu–Zn magnetite-rich Gossan Hill volcanic-hosted massive sulphide deposit, Western Australia: genesis of a multistage hydrothermal system. Economic Geology 97, 517–541.

Sillitoe, R.H., 1993. Giant and Bonanza Gold Deposits in the Epithermal Environment: Assessment of Potential Generic factors. In: Whiting, B.H., Hodgson, C.J. and Mason, R. (Eds). Giant Ore Deposits, Special Publication Number 2, Society of Economic Geologists, pp. 125–156.

Sibson, R.H., 1987. Earthquake rupturing as a hydrothermal mineralising agent. Geology 15, 701–704.

Sibson, R.H., Robert, F., Poulsen, K.H., 1988. High-angle reverse faults, fluid pressure cycling and mesothermal gold-quartz deposits. Geology 16, 551–555.

Taylor, D., Dalstra, H.J., Harding, A.E., Broadbent, G.C., Barley, M.E., 2001. Genesis of high-grade orebodies of the Hamersley Province, Western Australia. Economic Geology 96, 837–873.

Tóth, J., 1962. A theory of groundwater motion in small drainage basins in Central Alberta, Canada. Journal of Geophysical Research 67 (11), 4375–4387.

Tóth, J., 1963. A theoretical analysis of groundwater flow in small drainage basins. Journal of Geophysical Research 68 (16), 4795–4812.

Trendall, A.F., Blockley, J.G., 1970. The iron formations of the Precambrian Hamersley Group, Western Australia, with special reference to the associated Crocidolite. Geological Survey, Western Australian Bulletin 119, 365.

Tyler, I.M., 1991. The geology of the Sylvania Inlier and southeastern Hamersley Basin. Geological Survey, Western Australian Bulletin 138, 108.

Tyler, I.M., Thorne, A.M., 1990. The northern margin of the Capricorn Orogen, Western Australia—an example of an Early Proterozoic collision zone. Journal of Structural Geology 12, 685–701.

Upton, P., 1998. Modelling localization of deformation and fluid flow in a compressional orogen: implications for the Southern Alps of New Zealand. American Journal of Science 298, 296–323.

Upton, P., Koons, P.O., Chamberlain, C.P., 1995. Penetration of deformation-driven meteoric water into ductile rocks: isotopic and model observations from the Southern Alps, New Zealand. New Zealand Journal of Geology and Geophysics 38, 535–543.

Upton, P., Baxter, K., O'Brien, G.W., 1998. Coupled mechanical/fluid flow models of trap integrity and fault reactivation: application to the North West Shelf of Australia. Australian Petroleum Production and Exploration Association Journal 1998, 488–499.

Vermeer, P.A., de Borst, R., 1984. Non-associated plasticity for soils, concrete and rock. Heron 29, 1–62.

Webb, A.D., Dickens, G.R., Oliver, N.H.S., 2003. From banded iron-formation to iron ore: geochemical and mineralogical constraints from across the Hamersley Province, Western Australia. Chemical Geology 197, 215–251.